Title
Imaging cells and extracellular matrix in vivo by using second-harmonic generation and two-photon excited fluorescence

Journal
Proceedings of the National Academy of Sciences of the United States of America, 99(17)

ISSN
0027-8424

Authors
Zoumi, Aikaterini
Yeh, Alvin
Tromberg, Bruce J

Publication Date
2002-08-20

DOI
10.1073/pnas.172368799

Imaging cells and extracellular matrix *in vivo* by using second-harmonic generation and two-photon excited fluorescence

Aikaterini Zoumi*†, Alvin Yeh*, and Bruce J. Tromberg*†‡

*Laser Microbeam and Medical Program (LAMMP), Beckman Laser Institute, and †Center for Biomedical Engineering, University of California, Irvine, CA 92612

Communicated by Peter M. Rentzepis, University of California, Irvine, CA, June 20, 2002 (received for review January 20, 2002)

Multiphoton microscopy relies on nonlinear light–matter interactions to provide contrast and optical sectioning capability for high-resolution imaging. Most multiphoton microscopy studies in biological systems have relied on two-photon excited fluorescence (TPEF) to produce images. With increasing applications of multiphoton microscopy to thick-tissue "intravital" imaging, second-harmonic generation (SHG) from structural proteins has emerged as a potentially important new contrast mechanism. However, SHG is typically detected in transmission mode, thus limiting TPEF/SHG coregistration and its practical utility for *in vivo* thick-tissue applications. In this study, we use a broad range of excitation wavelengths (730–880 nm) to demonstrate that TPEF/SHG coregistration can easily be achieved in unstained tissues by using a simple backscattering geometry. The combined TPEF/SHG technique was applied to imaging a three-dimensional organotypic tissue model (RAFT). The structural and molecular origin of the image-forming signal from the various tissue constituents was determined by simultaneous spectroscopic measurements and confirming immunofluorescence staining. Our results show that at shorter excitation wavelengths (<800 nm), the signal emitted from the extracellular matrix (ECM) is a combination of SHG and TPEF from collagen, whereas at longer excitation wavelengths the ECM signal is exclusively due to SHG. Endogenous cellular signals are consistent with TPEF spectra of cofactors NAD(P)H and FAD at all excitation wavelengths. The reflected SHG intensity follows a quadratic dependence on the excitation power, decays exponentially with depth, and exhibits a spectral dependence in accordance with previous theoretical studies. The use of SHG and TPEF in combination provides complementary information that allows noninvasive, spatially localized *in vivo* characterization of cell–ECM interactions in unstained thick tissues.

Since its introduction by Denk *et al.* (1), two-photon excited fluorescence (TPEF) has been widely used for imaging structure and dynamic interactions in biological tissues (2–5). Although second-harmonic generation (SHG) in biological tissues was first demonstrated two decades ago (6–8), SHG has only recently been used for biological imaging applications (9–12). Because TPEF and SHG involve different contrast mechanisms, they can be used in tandem to provide complementary information regarding tissue structure and function. Specifically, SHG signals depend on the orientation, polarization, and local symmetry properties of chiral molecules, whereas TPEF results from the nonlinear excitation of molecular fluorescence.

The primary tissue constituent responsible for SHG is collagen (9, 13, 14), which is also a well documented source of tissue autofluorescence (4, 15). This fact has created uncertainty over whether the image-forming signal from two-photon excitation of collagen in biological tissues is TPEF or SHG and prompts further investigation into the precise origin of signal in the nonlinear microscopy of tissues. Detailed characterization of the collagen signal is particularly important because collagen is the most abundant structural protein in higher vertebrates, and structural modifications of the fibrillar matrix are associated with various physiologic processes such as aging, diabetes, wound healing, and cancer (16–18).

Most studies using nonlinear microscopic techniques for biological imaging have relied on TPEF. Recently, a combination of TPEF and SHG has been implemented for the study of cells stained with exogenous probes possessing large molecular anisotropy and second-order nonlinearity (10, 13, 19–21). Combined TPEF/SHG has been demonstrated for thin tissue sections (22), but not for the more practical case of thick, unstained living specimens because, although TPEF is measured in epi-illumination geometry, the forward propagating nature of the phase-coherent SHG signal seems to restrict SHG microscopy to a transmission mode of detection. In fact, under certain conditions, a significant amount of backscattering second-harmonic light can be generated at the interfaces between nonlinear and linear media (23–27). Reflected SHG signals provided the basis for the development of the first *in vivo* SHG tissue tomography (28, 29). The results obtained from this approach, however, were characterized by relatively poor resolution, lack of structural detail, and prohibitively long acquisition times (0.5–2.8 h).

In this study, we have modified a conventional TPEF laser-scanning microscope to observe the complete spectral content of multiphoton microscopy signals. Images and spectral measurements from two-photon excitation of an unstained organotypic tissue model (RAFT) are used to demonstrate the coregistration of SHG and TPEF from collagen across a broad excitation wavelength range in reflection geometry. The determination of the origin of signal from both cellular and ECM components is accomplished and shown to provide excellent contrast-enhancing opportunities for thick-tissue intravital imaging. Furthermore, the dependence of the detected SHG intensity on excitation wavelength and imaging depth is compared with a theoretical model and proposed as a means for extracting quantitative structural information from the tissue.

Materials and Methods

Preparation of Organotypic RAFT Tissue Model. The sample used in the experiments is an organotypic RAFT tissue model consisting of a basic polymerized collagen gel made up of type I rat-tail collagen and primary human neonatal dermal foreskin fibroblast cells. To construct the RAFT model, fibroblast cells were first isolated from donated human neonatal foreskin tissue and cultured in RPMI medium 1640 (Invitrogen) supplemented with 10% (vol/vol) FBS (Invitrogen). After reaching confluence, fibroblasts were trypsinized by using a 0.25% Trypsin/0.05% EDTA solution and added (10^5 cells per ml of collagen gel) to a mixture consisting of 65% type I rat-tail collagen at a concentration of 4 mg/ml in 0.02 N glacial acetic acid (RTTC, Collaborative Research), 20% 5× RPMI medium 1640 (Invitrogen) and 10% (vol/vol) reconstitution

Abbreviations: SHG, second-harmonic generation; TPEF, two-photon excited fluorescence; λ_{ex}, excitation wavelength; ECM, extracellular matrix; *z*, depth into the sample; PMT, photomultiplier tube.

‡To whom reprint requests should be addressed. E-mail: tromberg@bli.uci.edu.

 www.pnas.org/cgi/doi/10.1073/pnas.172368799

buffer consisting of 260 mM $NaHCO_3$ and 200 mM Hepes buffer in 0.05 N NaOH. Fibroblast-containing collagen mix (0.9 ml) was added into a well (≈18 mm in diameter) of a 24-well tissue culture plate (Costar), and the gel was allowed to set in a humidified incubator at 37°C with 7.5% CO_2 in air for a minimum of 2 h. Once solidified, the gel was released from its well by using a metal spatula and transferred to an imaging dish. Then the tissue was placed back in the humidified incubator until ready to be imaged. The sample used in the experiments herein was imaged 4 days after its preparation. During this time, the growth medium was changed every 2 days.

Immunofluorescence Staining Protocol. RAFT was initially stained with a mouse anti-human monoclonal antibody (MAB1340, Chemicon; 40 μg/ml), which has been shown to crossreact with rat-tail type I collagen, followed by a secondary $F(ab')_2$ fragment of goat anti-mouse IgG conjugated to Alexa Fluor 488 (a-11017, Molecular Probes; 20 μg/ml). Negative controls determined background fluorescence and no reactivity with collagen type I. Images of the immunostained RAFT were obtained to map the distribution of collagen fibers in the sample.

Experimental Layout. The two-photon imaging microscope used for this study consists of a mode-locked Ti:Sapphire laser (170-fs pulse width, 76 MHz repetition rate; Mira 900F, Coherent Radiation, Palo Alto, CA) pumped by a 5-W Verdi laser (Coherent Radiation). The beam exiting the laser is deflected into the back port of an inverted Axiovert 100 microscope (Zeiss) and scanned across the sample by a PC-controlled galvanometer-driven x–y scanner (Series 603X, Cambridge Technology, Watertown, MA). The beam is reflected by a short-pass 675-nm dichroic beam splitter (Chroma Technology, Brattleboro, VT) and focused onto the sample with a 63×, c-apochromat, N.A. = 1.2, water-immersion microscope objective (Zeiss). The average excitation power entering the microscope is approximately P = 60 mW (corresponding to 5 mW at the sample site) for all of the excitation wavelengths used. The TPEF and SHG signals from the sample are epi-collected, discriminated with the 675-nm short-pass dichroic mirror, transmitted through a short-pass 600-nm filter (CVI Laser, Livermore, CA) and detected by either a photomultiplier tube (PMT) or a spectrograph.

Two-dimensional (x–y plane) images (256 × 256 pixels) are acquired from various depths (z) into the sample at a rate of one frame per s (pixel dwell time of 16 μs/pixel) with a single-photon counting PMT (R7400P, Hamamatsu, Bridgewater, NJ), covering an area of 35 × 35 μm^2 for the 63× microscope objective. Resolution is ≈0.4 μm and 1 μm in the x–y and z image planes, respectively. Unless otherwise specified, an SBG39 wide-pass (322–654 nm) blue-green emission filter (CVI, Albuquerque, NM) is placed in front of the PMT. Each acquired image is typically integrated for 10 s.

Spectral measurements are obtained with a SpectraPro-150 spectrograph, which is directly coupled to the side port of the microscope by a relay lens. The spectrograph has a 300 grooves per mm grating blazed at 500 nm (Acton Research, Acton, MA), and is equipped with a high dynamic range MicroMax:512BFT CCD camera (Princeton Instruments, Trenton, NJ) which is controlled by an ST-133 Controller (Princeton Instruments). The camera has a 512 × 512-pixel imaging array, where each pixel is a 13 × 13 μm square. The entrance slit of the spectrograph is set to a width of 0.5 mm throughout the experiments. The spectrograph and camera settings are PC-controlled through commercially available software (WINSPEC/32 v. 2.4.6.6, Roper Scientific, Trenton, NJ). The CCD temperature is maintained to the minimum possible temperature (−45°C) for all of the experiments to ensure low dark noise. The spectra acquisition time, Δt, is 60 s.

Switching between imaging and spectra acquisition is achieved by means of changing the position of a built-in microscope mirror. When two-photon images and spectra are both obtained from the sample, the two-photon images are acquired and stored, immediately followed by emission spectra acquisition from the same depth, z, into the sample. Dark noise spectra are subtracted from the acquired sample spectra. Spectral data are imported into MICROSOFT EXCEL 2000 (Microsoft) for analysis and display. Acquired images are color-coded by using IPLAB SPECTRUM image-processing software (Scanalytics, Fairfax, VA).

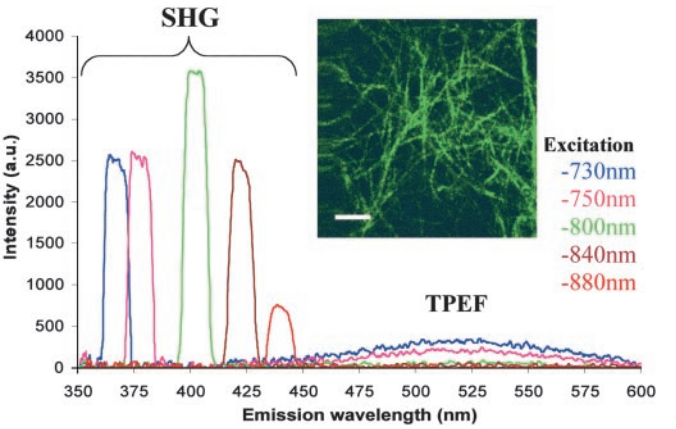

Fig. 1. Emission spectra obtained from RAFT collagen for λ_{ex} = 730, 750, 800, 840, and 880 nm for acquisition time Δt = 60 s. Each spectrum is the average of five measurements acquired at different x–y locations of the sample surface (z = 0 μm). Spectral data obtained for slightly different values of excitation power, P, (namely, 54.2 mW for λ_{ex} = 730 nm, 57.3 mW for λ_{ex} = 750 nm, 60.1 mW for λ_{ex} = 800 nm, 64.1 mW for λ_{ex} = 840 nm, and 60.3 mW for λ_{ex} = 880 nm) have been normalized to P = 60.1 mW by using the quadratic dependence of SHG intensity on the excitation power, which was experimentally validated. The spectra have been corrected for the spectral dependence of the microscope objective transmission, the spectrograph grating efficiency, and the transmission of the optical components (filters, dichroic mirrors, etc.) in the optical path of the two-photon system. *Inset* shows an image obtained from RAFT collagen for λ_{ex} = 800 nm at z = 0 μm. (Bar = 5 μm.)

Results and Discussion

Origin of Image-Forming Signal for Collagen. To determine the origin of signal (TPEF or SHG) from collagen in the RAFT the Ti:Sapphire laser was tuned to various excitation wavelengths, λ_{ex}, throughout its tuning range (namely, 730, 750, 800, 840, and 880 nm), and two-photon images and spectra were acquired from the sample surface (z = 0 μm) when collagen alone (i.e., in the absence of fibroblasts) could be visualized. A representative two-photon image acquired for λ_{ex} = 800 nm is shown in Fig. 1 *Inset*, where structural details of the sample can be readily distinguished. The image displays a network of filaments that correspond to collagen fibers with diameters of ≈0.5 μm. No cells can be visualized in this image. Fig. 1 also depicts collagen emission spectra acquired from the RAFT surface (z = 0 μm) for λ_{ex} = 730, 750, 800, 840, and 880 nm. Each emission spectrum has been averaged across five measurements acquired at different x–y locations of the sample surface to account for variations in the spectral intensities due to possible nonuniformity of the collagen content. All measurements were done in triplicate. The emission spectra of Fig. 1 have been corrected for the spectral dependence of the microscope objective transmission, the spectrograph grating efficiency, and the transmission of the optical components (filters, dichroic mirrors, etc.) in the optical path of the two-photon system by use of a National Institute of Standards and Technology (NIST)-calibrated Hg(Ar) lamp (Oriel, Stratford, CT).

For all of the excitation wavelengths used, the emission spectra reveal strong SHG signals manifested by a narrow peak at half the excitation wavelength and a bandwidth (full width at half-maximum) in accordance with the excitation laser spectral width.

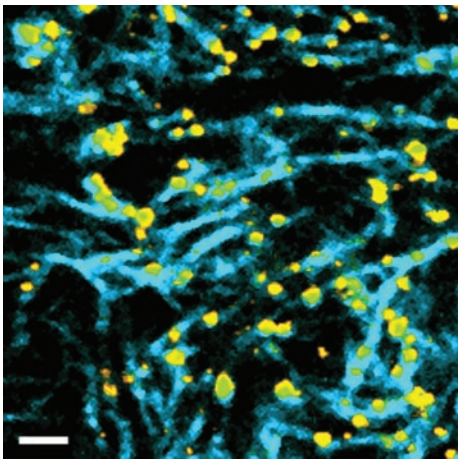

Fig. 2. Color-coded image of immunostained collagen fibers in the RAFT. The image is an overlay of two images obtained from the same sample site by using an SBG39 (322–654 nm) wide-pass emission filter and a 520/40 nm bandpass emission filter for λ_{ex} = 800 nm, and P = 60 mW. Collagen fibers are shown in cyan, and the spotted staining pattern of the antibody is shown in yellow. (Bar = 3 μm.)

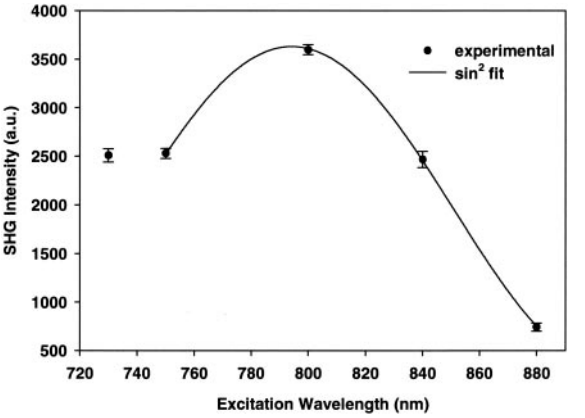

Fig. 3. Spectral dependence of SHG intensity. The experimental data correspond to the SHG peak intensity values obtained from the corrected spectra in Fig. 1. Each point is the average of five measurements acquired at different x–y locations of the sample surface. Each measurement was performed in triplicate. The solid line corresponds to a nonlinear regression fit of the form $I_{SHG} = a + b \sin^2(2\pi\lambda/c + d)$.

For each examined λ_{ex}, the spectrally detected SHG intensity exhibited a quadratic dependence on the laser power, which is consistent with second-order nonlinear frequency conversion. Although SHG is still the dominant signal for λ_{ex} = 730 nm and λ_{ex} = 750 nm, the emission spectra also display a broad feature from 410 to 600 nm, with a maximum at 525 nm, that corresponds to TPEF from collagen. The TPEF intensity is higher for λ_{ex} = 730 nm than for λ_{ex} = 750 nm. No TPEF signal from collagen was detected for λ_{ex} = 800, 840, and 880 nm.

Collagen Mapping by Immunofluorescence Staining. To confirm that the filamentous structures in the two-photon images obtained from the RAFT correspond to collagen fibers, images were obtained from a RAFT sample stained with type I collagen specific antibody (MAB1340, Chemicon) for λ_{ex} = 800 nm by using two different emission filters in front of the PMT. Specifically, images were obtained with an SBG39 wide-pass (322–654 nm) and a 520/40 nm bandpass emission filter, and were overlaid by using IPLAB SPECTRUM image-processing software (Scanalytics). Fig. 2 illustrates the resulting color-coded image, which displays SHG signals in cyan and antibody fluorescence in yellow. The immunostaining pattern reveals that the fibers in the RAFT correspond to collagen, and thus the TPEF and SHG signals indeed originate from type I collagen.

Spectral Dependence of Reflected SHG Intensity. Inspection of the emission spectra depicted in Fig. 1 reveals a spectral dependence of the peak SHG intensity. Fig. 3 shows a plot of the SHG intensity values obtained from the spectra in Fig. 1 as a function of the excitation wavelength. The SHG intensity is maximum for λ_{ex} = 800 nm, and decreases at longer and shorter wavelengths. Previous studies demonstrating SHG from type I collagen in transmission mode have shown no SHG intensity variation within a 766- to 1,064-nm excitation wavelength range (9). To our knowledge, no experimental studies have been done on the spectral dependence of the SHG intensity detected from collagen in reflection geometry.

Theoretical studies (23, 25–27) have shown that the second-harmonic field generated by a nonlinear medium embedded in a linear medium is a composite function of second-harmonic light reflected from a layer of about one wavelength thick at the interface between the linear and the nonlinear medium, and second-harmonic light generated in the bulk of the nonlinear medium, which propagates predominantly in the forward direction. In contrast to the transmission mode of detection, the reflected SHG from the interface can have a significant contribution to the output SHG intensity measured in backscattering mode (23). Theoretical simulations of the reflected SHG intensity generated by a slab of nonlinear medium of thickness L embedded in a linear medium (26) predict a reflected SHG intensity profile that oscillates with the excitation wavelength as a result of the interference of the two SHG waves reflected by the interfaces at $z = 0$ and $z = L$. The SHG reflected from the second interface ($z = L$) is generated by the SHG wave that is transmitted from the first interface ($z = 0$) through the bulk of the slab.

According to this formulation, the reflected SHG signal measured from the RAFT is the contribution of the SHG signal reflected from a thin layer at the RAFT surface and the transmitted SHG waves generated at various planes, which propagate a distance L into the sample before loss of coherence caused by scattering. The transmitted SHG signals from various depths, z, exhibit interference described by the factor $\sin^2(2\pi\Delta nL/\lambda_{ex})$, where Δn is the dispersion of the RAFT, and λ_{ex} is the fundamental wavelength (30). The distance L represents the sample scattering length, l_{scat}, because, due to the coherence of the SHG process, the measured SHG intensity is determined by ballistic photons that carry the coherent information from the medium (28). Thus, l_{scat} represents the mean distance through which coherently interfering SHG waves can travel before scattering. On the basis of this analysis, a four-parameter $\sin^2$ function fit of the form $I_{SHG} = a + b \sin^2(2\pi\lambda_{ex}/c + d)$ was applied to the experimental data and is shown in Fig. 3 as a solid line. A significant deviation from the model was observed for the SHG signal at the excitation wavelength of 730 nm. Here, the SHG intensity is likely to be higher than the value predicted from the fit because of resonance enhancement that occurs when the collagen excited state is close to the SHG wavelength.

The results presented herein reveal the existence of an optimal excitation wavelength for *in vivo* SHG imaging of the ECM that is not at resonance, which suggests that photobleaching and photodamage effects associated with two-photon absorption can be eliminated in SHG imaging. Moreover, the dependence of the interference factor $\sin^2(2\pi\Delta nl_{scat}/\lambda_{ex})$ on sample properties, such as dispersion and scattering length, suggests the potential use of the SHG intensity spectral dependence for the extraction of quantitative tissue information. For example, it has been estimated that the dispersion, Δn, of the rat tail tendon for λ_{ex} = 1,064 nm is 0.026 (14). Assuming that the $\sin^2$ function describing the experimentally observed spectral dependence of the SHG intensity is equal to the

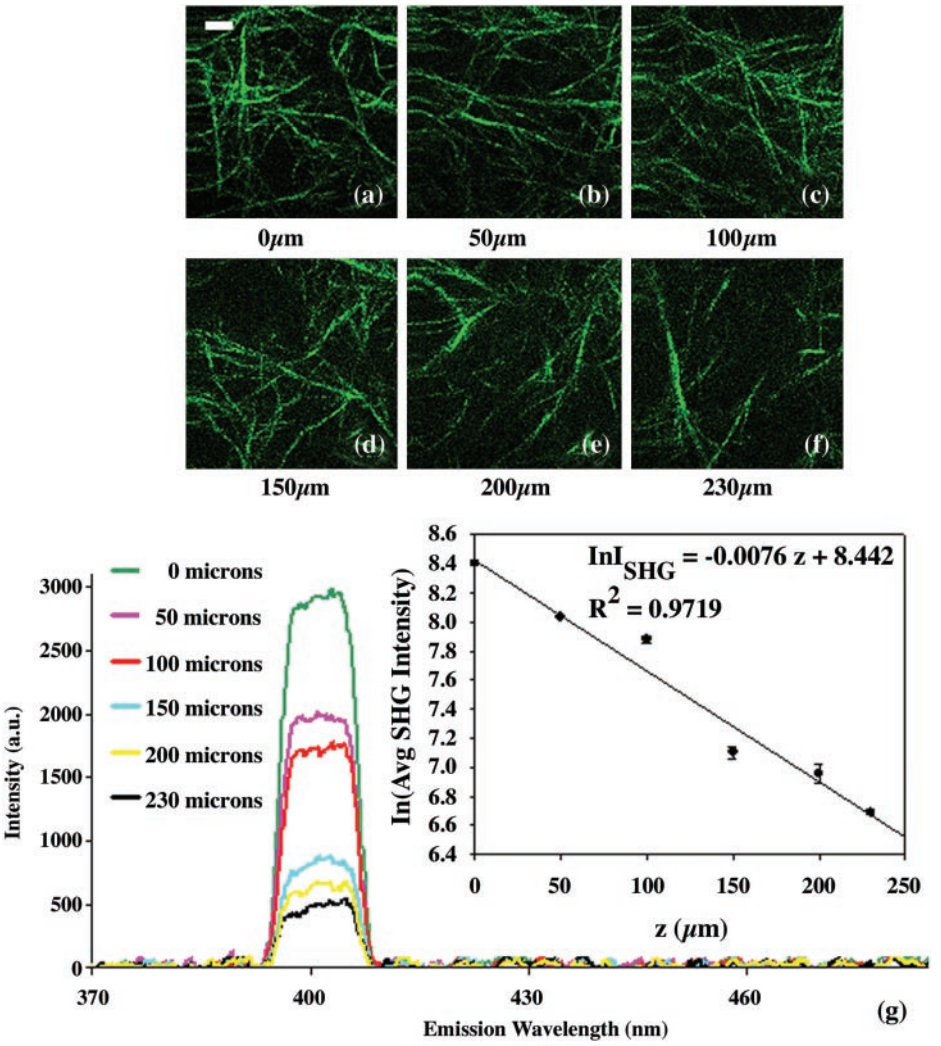

Fig. 4. SHG images from RAFT collagen at depths of 0, 50, 100, 150, 200, and 230 μm for λ_{ex} = 800 nm and P = 60 mW (*a–f*). (Bar = 5 μm.) The corresponding spectra for Δt = 60 s are shown in *g*. (*g Inset*) Plot of the log of SHG intensity vs. depth, z (μm).

interference factor $\sin^2(2\pi\Delta n l_{scat}/\lambda_{ex})$, we can estimate the RAFT scattering length as $l_{scat} = (\lambda_{ex}/2\pi\Delta n)(2\pi\lambda_{ex}/c + d)$, which for λ_{ex} = 1,064 nm, Δn = 0.026, c = 453.7, and d = 6.28 yields $l_{scat} \approx$ 137 μm. This value is in good agreement with previous near-infrared spectroscopic measurements of $l_{scat} \approx$ 100–150 μm in nonkeratinized epithelial tissue (31).

High-Resolution Reflectance Imaging Deep Inside Tissue. To demonstrate our system capability to generate high-resolution structural images deep inside highly scattering tissues two-photon images were obtained at various depths, z, into the RAFT ranging from 0 to 230 μm, which is the working distance of the microscope objective. Fig. 4 *a–f* illustrates two-photon images of RAFT collagen at depths of 0, 50, 100, 150, 200, and 230 μm, for λ_{ex} = 800 nm, which is the optimal excitation wavelength for SHG imaging. It is apparent that detailed structural information can be deduced from the images throughout the examined depth range. The signal progressively degrades with increasing depth and fewer collagen fibers can be resolved in the images. However, the maximum imaging depth reached here is only limited by the working distance of the microscope objective and the low value of excitation power used (approximately 5 mW at the sample site). Previous studies using SHG imaging in reflection geometry to obtain structural information deep inside tissue (28, 29) are characterized by long acquisition times (0.5–2.8 h) and poor resolution even for excitation powers as high as 80 mW at the sample (29).

To investigate the dependence of the SHG intensity on imaging depth in turbid tissues, spectra corresponding to the images shown in Fig. 4 *a–f* were acquired and are shown in Fig. 4*g*. The *Inset* in Fig. 4*g* shows a plot of the natural logarithm of the spectrally detected SHG peak intensity versus depth, z, for λ_{ex} = 800 nm. The SHG intensity at each depth in Fig. 4*g* is the average of five measurements at different x–y locations in the same z plane. The experiment was repeated three times to ensure the reproducibility of the results. The SHG signal decays with depth because of absorption and scattering in the sample. Multiple light scattering decreases the intensity of ballistic excitation photons reaching the focus area, limiting the number of SHG photons generated in the tissue. The SHG intensity, I_{SHG}, decays as a function of depth, z, according to: $(I_{SHG})^z = (I_{SHG})^{z=0} \exp(-Az)$, where A is an attenuation coefficient that is a function of the sample absorption and scattering properties at both the excitation and emission (SHG) wavelengths. The inverse of A yields an attenuation length, $l_{att} \approx 132$ μm, that is a composite optical property of the RAFT and approximates $l_{scat} \approx$ 137 μm, which was estimated by using the spectral dependence of the SHG intensity. These findings suggest the potential use of the SHG depth-dependent decay and the spectral dependence of the SHG intensity as sensitive tools for obtaining quantitative tissue structural information. However, further work is necessary to determine the precise physical meaning of these composite parameters.

Origin of Image-Forming Signal for Cells. To investigate the origin of endogenous signal from the fibroblast cells in the RAFT, two-

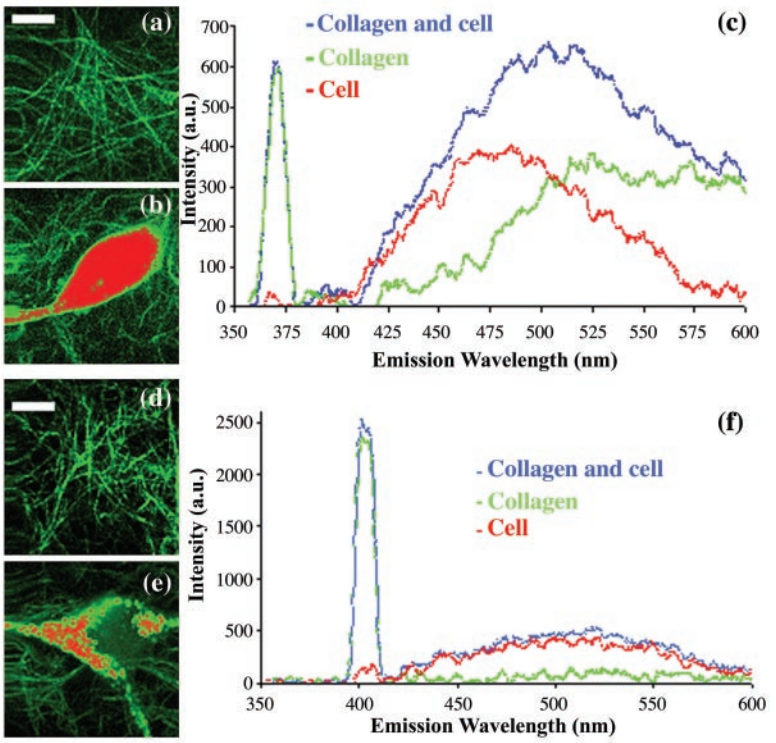

Fig. 5. Combined SHG/TPEF images from RAFT collagen only (*a*), and for collagen and cell (*b*) for $\lambda_{ex} = 730$ nm, $P = 54.2$ mW, $z = 88$ μm. (Bar = 8 μm.) The corresponding emission spectra ($\Delta t = 60$ s) are shown in *c*. SHG image from RAFT collagen only (*d*), and combined SHG/TPEF image for collagen and cell (*e*) for $\lambda_{ex} = 800$ nm, $P = 60$ mW, $z = 40$ μm in *d*, and $z = 36$ μm in *e*. (Bar = 8 μm.) The corresponding emission spectra ($\Delta t = 60$ s) are depicted in *f*.

photon images and the corresponding emission spectra were acquired for λ_{ex} = 730, 750, 800, 840, and 800 nm across a broad emission region (350–600 nm) in two cases: when both collagen and fibroblasts could be visualized in the images, and when collagen alone was in the field of view. Representative images and emission spectra for $\lambda_{ex} = 730$ and 800 nm are shown in Fig. 5. For $\lambda_{ex} = 730$ nm (Fig. 5 *a–c*), the collagen emission spectrum (Fig. 5*c*, green) exhibits a 365-nm SHG peak followed by a broad peak in the 410- to 600-nm region with a maximum at 525 nm because of collagen autofluorescence. The emission spectrum from both collagen and a fibroblast cell (Fig. 5*c*, blue) displays the 365-nm SHG signal, and a broad peak with a maximum at 510 nm, resulting from both collagen and fibroblast autofluorescence. Subtraction of the former from the latter spectrum yields the TPEF signal resulting exclusively from cellular autofluorescence (Fig. 5*c*, red). The cellular TPEF signal covers a broad emission region between 400 and 600 nm, with a maximum at 480 nm. This signal is consistent with the emission of NAD(P)H (32). This finding was also observed for $\lambda_{ex} = 750$ nm.

For $\lambda_{ex} = 800$ nm (Fig. 5 *d–f*), the emission spectrum from both collagen and a fibroblast cell (Fig. 5*f*, blue) consists of a SHG peak at 400 nm, and a broad peak between 410 and 600 nm with a maximum at 520 nm. The spectrum for collagen alone (Fig. 5*f*, green) exhibits solely the 400-nm SHG peak. Autofluorescence from the cell alone is obtained by subtraction of the two emission spectra above (Fig. 5*f*, red) and manifests a broad emission covering the region from 420 to 600 nm, with a maximum at 520 nm. The red-shifting of the cellular TPEF as compared with that observed for $\lambda_{ex} = 730$ nm, suggests that at $\lambda_{ex} = 800$ nm, TPEF from the cells is probably a combination of fluorescence from NAD(P)H and flavin compounds, whereas the latter are not sufficiently excited at 730 nm (33). In contrast to the TPEF signal obtained from the RAFT for λ_{ex} = 730 nm, which consists of both fibroblast and

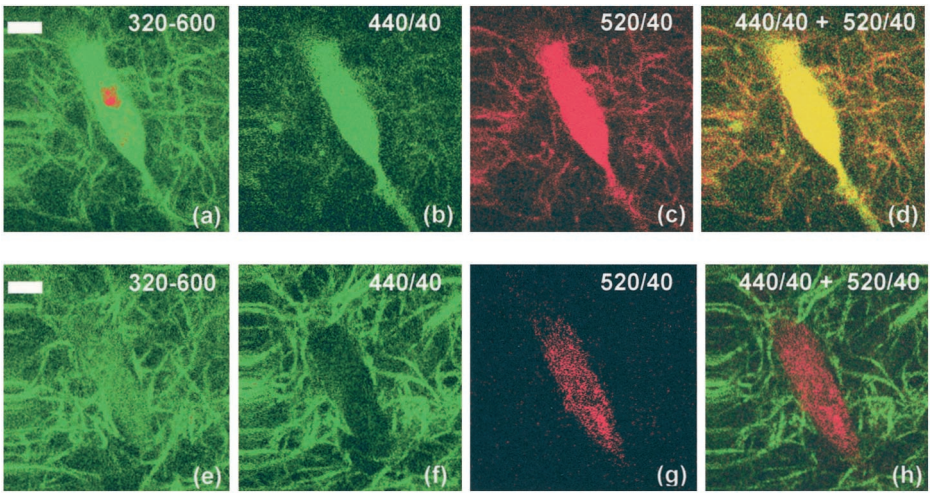

Fig. 6. (*Upper*) Images of the RAFT (collagen and fibroblast) acquired at $\lambda_{ex} = 750$ nm, for P = 60.2 mW, at the same focal plane $z = 80$ μm (*a–d*). Images were obtained from the same sample site by using different filters in front of the PMT: (*a*) An SBG39 filter (320–620 nm); (*b*) a 440/40 nm bandpass filter; and (*c*) a 520/40 nm bandpass filter. Image in *d* was obtained by overlaying the images in *b* and *c*. (*Lower*) Images from the same site of the RAFT (collagen and fibroblast) acquired at $\lambda_{ex} = 840$ nm, for $P = 64.1$ mW, at the same focal plane z = 162 μm (*e–h*). Images *e–g* were obtained by using the same filters as in *a–c*. Image in *h* was obtained by overlaying the images in *f* and *g*. (Bar = 6 μm.)

collagen autofluorescence, at λ_{ex} = 800 nm the TPEF signal is observed exclusively due to cellular autofluorescence and the SHG signal originates from collagen. Similar observations were made for λ_{ex} = 840 and 880 nm.

Contrast Enhancement Facilitated by Determination of Image-Forming Signal. Achieving high contrast and high spatial resolution is one of the primary goals for *in vivo* functional imaging. Understanding the origin of the image-forming signal (TPEF or SHG) for the different tissue constituents can provide a stratagem for enhancing contrast in TPEF/SHG imaging of biological tissues. Specifically, selection of longer excitation wavelengths results in signals from the cellular and ECM tissue constituents that are spectrally distinct and can be easily separated by use of optical filters or by dual-channel detection. Fig. 6 illustrates an example of the use of this approach to separate the signals from a cell and the ECM. Images were obtained from the same sample site at the same focal plane in the RAFT by using different emission filters in front of the PMT: (*i*) An SBG39 filter (320–620 nm), (*ii*) a 440/40 nm bandpass filter (for green-coded images), and (*iii*) a 520/40 nm bandpass filter (for red-coded images). At short excitation wavelengths (750 nm, Fig. 6 *a–d*) where TPEF is a combination of cellular and matrix fluorescence, the use of narrow bandpass emission filters does not suffice to separate one signal from the other. Therefore, overlaying the green (Fig. 6*b*) and red (Fig. 6*c*) images results in an image displaying both collagen and cellular signals in yellow (Fig. 6*d*). In contrast, for longer excitation wavelengths (840 nm, Fig. 6 *e–h*), where the only signal associated with collagen is SHG, and TPEF originates exclusively from the cell, use of the same optical filters allows complete isolation of the cellular and the matrix signals. In this case, overlaying the green (Fig. 6*f*) and red (Fig. 6*g*) images results in a high-contrast image (Fig. 6*h*), where collagen and cellular signals can be selectively visualized. This finding is of significance for noninvasive, spatially localized *in vivo* characterization of cell–ECM interactions and pathology.

Conclusions

We have demonstrated the coregistration of TPEF and SHG in an unstained three-dimensional organotypic RAFT tissue model by using a simple backscattering geometry. The origin of the image-forming signal (TPEF and/or SHG) from the various RAFT constituents was determined by spectral measurements across a broad range of excitation wavelengths (730–880 nm). Our results indicate that for excitation wavelengths shorter than 800 nm the signal from the ECM is a combination of SHG and TPEF from collagen, whereas at longer excitation wavelengths the ECM signal is exclusively due to SHG. Cellular signals are due to TPEF at all excitation wavelengths. Understanding the origin of the image-forming signal for the different tissue constituents can provide a means for enhancing contrast between cellular and ECM components in TPEF/SHG imaging of biological tissues. Our findings also suggest that the exponential depth-dependent decay and the spectral dependence of the reflected SHG intensity can serve as models for obtaining quantitative tissue information such as dispersion and scattering length that can potentially be used for the characterization of normal and diseased tissue states. The combined use of TPEF and SHG in reflection geometry provides complementary information that allows noninvasive, spatially localized *in vivo* characterization of cell–ECM interactions and pathology.

We thank T. B. Krasieva and C.-H. Sun for helpful discussions and technical assistance. This work was supported by the National Institutes of Health Laser Microbeam and Medical Program (P41RR-01192), the Department of Energy (DOE DE-FG03–91ER61227), Air Force Office of Scientific Research Medical Free Electron Laser Program (F49620–00-1–0371), and National Institutes of Health, Carcinogenesis Training Grant CA-09054 (to A.Y.).

1. Denk, W., Strickler, J. H. & Webb, W. W. (1990) *Science* **248,** 73–76.
2. Masters, B. R., So, P. T. C. & Gratton, E. (1998) *Lasers Med. Sci.* **13,** 196–203.
3. Masters, B. R. & So, P. T. C. (2001) *Opt. Express* **8,** 2–10.
4. Agarwal, A., Coleno, M. L., Wallace, V. P., Wu, W. Y., Sun, C. H., Tromberg, B. J. & George, S. C. (2001) *Tissue Eng.* **7,** 191–202.
5. Diaspro, A. & Robello, M. (2000) *J. Photochem. Photobiol. B* **55,** 1–8.
6. Freund, I., Deutsch, M. & Sprecher, A. (1986) *Biophys. J.* **50,** 693–712.
7. Fine, S. & Hansen, W. P. (1971) *Appl. Opt.* **10,** 2350–2353.
8. Roth, S. & Freund, I. (1980) *Opt. Commun.* **33,** 292–296.
9. Georgiou, E., Theodossiou, T., Hovhannisyan, V., Politopoulos, K., Rapti, G. S. & Yova, D. (2000) *Opt. Commun.* **176,** 253–260.
10. Campagnola, P. J., Wei, M. D., Lewis, A. & Loew, L. M. (1999) *Biophys. J.* **77,** 3341–3349.
11. Gauderon, R., Lukins, P. B. & Sheppard, C. J. R. (1998) *Opt. Lett.* **23,** 1209–1211.
12. Moreaux, L., Sandre, O. & Mertz, J. (2000) *J. Opt. Soc. Am. B* **17,** 1685–1694.
13. Campagnola, P. J., Clark, H. A., Mohler, W. A., Lewis, A. & Loew, L. M. (2001) *J. Biomed. Opt.* **6,** 277–286.
14. Roth, S. & Freund, I. (1981) *Biopolymers* **20,** 1271–1290.
15. Masters, B. R. & So, P. T. C. (1999) *Microsc. Microanal.* **5,** 282–289.
16. Kim, B. M., Eichler, J., Reiser, K. M., Rubenchik, A. M. & Da Silva, L. B. (2000) *Lasers Surg. Med.* **27,** 329–335.
17. Tanaka, S., Avigad, G., Brodsky, B. & Eikenberry, E. F. (1988) *J. Mol. Biol.* **203,** 495–505.
18. Odetti, P., Pronzato, M. A., Noberasco, G., Cosso, L., Traverso, N., Cottalasso, D. & Marinari, U. M. (1994) *Lab. Invest.* **70,** 61–67.
19. Gauderon, R., Lukins, P. B. & Sheppard, C. J. (2001) *Micron* **32,** 691–700.
20. Moreaux, L., Sandre, O., Blanchard-Desce, M. & Mertz, J. (2000) *Opt. Lett.* **25,** 320–322.
21. Moreaux, L., Sandre, O., Charpak, S., Blanchard-Desce, M. & Mertz, J. (2001) *Biophys. J.* **80,** 1568–1574.
22. Campagnola, P. J., Millard, A. C., Terasaki, M., Hoppe, P. E., Malone, C. J. & Mohler, W. A. (2002) *Biophys. J.* **82,** 493–508.
23. Shen, Y. R. (1984) *Principles of Nonlinear Optics* (Wiley, New York).
24. Williams, R., Zipfel, W. R. & Webb, W. W. (2001) *Curr. Opin. Chem. Biol.* **5,** 603–608.
25. Bloembergen, N. (1996) *Nonlinear Optics* (World Scientific, Teaneck, NJ).
26. Le Calvez, A., Freysz, E. & Ducasse, A. (1998) *Opt. Commun.* **145,** 135–140.
27. Bloembergen, N. & Pershan, P. S. (1962) *Phys. Rev.* **128,** 606–622.
28. Guo, Y. C., Ho, P. P., Savage, H., Harris, D., Sacks, P., Schantz, S., Liu, F., Zhadin, N. & Alfano, R. R. (1997) *Opt. Lett.* **22,** 1323–1325.
29. Guo, Y., Savage, H. E., Liu, F., Schantz, S. P., Ho, P. P. & Alfano, R. R. (1999) *Proc. Natl. Acad. Sci. USA* **96,** 10854–10856.
30. Yariv, A. (1991) *Optical Electronics* (Saunders, Philadelphia).
31. Hornung, R., Pham, T. H., Keefe, K. A., Berns, M. W., Tadir, Y. & Tromberg, B. J. (1999) *Hum. Reprod.* **14,** 2908–2916.
32. Piston, D. W., Masters, B. R. & Webb, W. W. (1995) *J. Microsc.* **178,** 20–27.
33. Richards-Kortum, R. & Sevick-Muraca, E. (1996) *Annu. Rev. Phys. Chem.* **47,** 555–606.